INTERNATIONAL JOURNAL FOR NUMERICAL METHODS IN FLUIDS
Int. J. Numer. Meth. Fluids 2007; **53**:1863–1886
Published online 25 October 2006 in Wiley InterScience (www.interscience.wiley.com). DOI: 10.1002/fld.1386

Direct sensitivity analysis for smooth unsteady compressible flows using complex differentiation

Shang-Yi Lu[1] and Pierre Sagaut[2,*,†]

[1]*Department of Mathematics, National University of Singapore, Singapore 117543, Singapore*
[2]*Laboratoire de Modélisation en Mécanique, Université Pierre et Marie Curie - Paris 6, 4, place Jussieu, case 162, Paris 75252 cedex 5, France*

SUMMARY

A method for the direct computation of the instantaneous sensitivities of unsteady compressible flows is proposed. It is based on the complex differentiation of the full compressible Navier–Stokes equations and does not require the storage of the unsteady flow solution to be differentiated. The method does not rely on any assumption on the basic Navier–Stokes solver, and can therefore be implemented in a straightforward way. The method is assessed on several cases, including a two-dimensional subsonic mixing layer. It is observed that the sensitivity patterns can be interpreted thanks to Kovasznay's decomposition for perturbations in a compressible flow. Copyright © 2006 John Wiley & Sons, Ltd.

Received 21 June 2006; Revised 29 August 2006; Accepted 6 September 2006

KEY WORDS: numerical method; compressible flows; sensitivity analysis

1. INTRODUCTION

The sensitivity of a compressible flow with respect to disturbances is a topic of major interest in fluid dynamics. It can be interpreted as a measure of its receptivity to perturbations, and its knowledge is of central interest for many purposes like stability analysis and flow control. Highly sensitive flows can be deeply modified by small disturbances, and can therefore be controlled with low-energy devices and/or small changes in the geometry of solid bodies, while unsensitive flows are very difficult to control, since they are robust with respect to external perturbations.

Sensitivity analysis [1] is commonly carried out using the linear stability theory [2, 3], and is therefore usually restricted to simplified cases which can be handled using the classical theoretical tools, such as normal mode decomposition. Another way to gain information dealing with the

*Correspondence to: Pierre Sagaut, Laboratoire de Modélisation en Mécanique, Université Pierre et Marie Curie - Paris 6, 4, place Jussieu, case 162, Paris 75252 cedex 5, France.
†E-mail: pierre.sagaut@upmc.fr

sensitivity of a flow is to carry out a 'brut force' analysis, i.e. to generate abacuses performing a large number of experiments with different operational conditions and comparing flow solutions. This method has no restriction with respect to the flow complexity, but is very expensive.

It is also possible to address the sensitivity issue using the approaches belonging to the differentiation method family. Here, the purpose is to compute the gradient of the solution with respect to a given flow parameter. A large number of mathematical tools related to this approach exist, which have been applied within the shape optimization framework, a few of them having been recently employed for active flow control purpose. The sensitivity of the flow is interpreted as the derivatives of the solution. The key element in these approaches is the computation of the solution derivatives. The most general approaches are based on the dual approach and require to solve the adjoint problem with *ad hoc* boundary conditions. Despite this method is very powerful, its use is still usually restricted to steady flows, because it requires the storage of the unsteady solution. This problem can be (at least partially) alleviated using surrogates for the direct unsteady solution or incomplete gradient approaches.

The present paper deals with an approach that makes it possible to compute at the same time in a single run the usual flow solution and its instantaneous sensitivity for unsteady solution, without the need for storing the solution. It is based on the complex differentiation approach, and necessitates a trivial modification of common Navier–Stokes solvers. It can therefore be implemented in a straightforward manner. The complex differentiation has been demonstrated to be much more accurate that the usual finite-difference approach. Another advantage is that the direct computation of instantaneous sensitivities of instantaneous flow events (e.g. vortices, acoustic waves) provides the user with a deep insight into the flow physics and may be of major interest to design flow control strategies/devices.

To the knowledge of the authors, it is the first time that the full sensitivity of the compressible unsteady flows is computed using the complex variable approach.

The paper is organized as follows. Section 2 presents the governing equations and introduces the sensitivity variables for the compressible Navier–Stokes equations. Full exact governing equations for these variables are also given. The complex differentiation approach is presented in Section 3 along with the related direct computation of the unsteady sensitivity field. The main elements of the numerical method used to solve the Navier–Stokes equations are given in Section 5. The proposed method is illustrated using simple but meaningful examples in Section 6.

2. GOVERNING EQUATIONS AND SENSITIVITY VARIABLES

2.1. Governing equations

The three-dimensional Navier–Stokes equations in terms of the pression p, the velocity $u=(u_1, u_2, u_3)$ and the entropy s are as follows, using the notation of repeated indices:

$$\begin{aligned} \frac{\partial p}{\partial t}+u_i\frac{\partial p}{\partial x_i}+p\gamma\frac{\partial u_i}{\partial x_i}-\frac{p}{C_v}\left(\frac{\partial s}{\partial t}+u_i\frac{\partial s}{\partial x_i}\right)&=0\\ \rho\left(\frac{\partial u_i}{\partial t}+u_j\frac{\partial u_i}{\partial x_j}\right)+\frac{\partial p}{\partial x_i}-\frac{\partial \tau_{ij}}{\partial x_j}&=0\\ \frac{\partial s}{\partial t}+u_i\frac{\partial s}{\partial x_i}+\frac{R}{p}\left(\frac{\partial q_i}{\partial x_i}+\Phi\right)&=0 \end{aligned} \tag{1}$$

DOI: 10.1002/fld

where the viscous tensor is defined as

$$\tau_{ij} = 2\mu s_{ij} + \lambda \frac{\partial u_k}{\partial x_k} \delta_{ij} \tag{2}$$

and the tensor

$$s_{ij} = \frac{1}{2}\left(\frac{\partial u_i}{\partial x_j} + \frac{\partial u_j}{\partial x_i}\right) \tag{3}$$

with $3\lambda + 2\mu = 0$. We will refer to the thermally ideal gas throughout this paper:

$$p = \rho RT \tag{4}$$

The propagation of heat is given by Fourier's law

$$q_j = -\kappa \frac{\partial T}{\partial x_j} \tag{5}$$

where T is the temperature (in kelvins K) and κ the thermal conductivity. The constant κ can be expressed in terms of the dynamic viscosity μ by

$$\kappa = \frac{\mu C_p}{Pr} \tag{6}$$

where Pr is the Prandtl number, and C_p the specific heat at constant pressure, C_v the specific heat at constant volume, and the ratio of the specific heats is denoted by γ:

$$\gamma = \frac{C_p}{C_v} \tag{7}$$

The speed of sound, c, is given by

$$c = \sqrt{\gamma RT} \tag{8}$$

Finally, viscous dissipation is denoted by

$$\Phi = \tau_{ij} s_{ij} \tag{9}$$

These equations, once discretized on a suitable grid, allows the direct numerical simulation of a compressible flow and thus describe all non-stationary dynamics that results. They also allow us to describe the propagation of acoustic waves given that the grid resolution is adapted to the problem.

2.2. *Sensitivity variables*

Let us consider the case if we are interested in analysing the sensitivity of the computed solution with respect to a scalar real parameter α. The parameter α can be related to any variables involved in the numerical model: boundary conditions, initial condition, numerical scheme coefficient or physical parameters such as the Reynolds number and the Mach number. All flow variables can be formally rewritten as function of space, time and α:

$$\phi = \phi(x, t; \alpha), \quad \phi = u, s, p, \rho, T \tag{10}$$

DOI: 10.1002/fld

The sensitivity variables u_i^δ, s^δ, p^δ, ρ^δ and T^δ about the state $\alpha=\alpha_0$ are defined as

$$\phi^\delta(x,t;\alpha_0)\equiv\frac{\partial\phi}{\partial\alpha}(x,t;\alpha=\alpha_0),\quad \phi=u,s,p,\rho,T \tag{11}$$

The variable ϕ^δ is related to the sensitivity of ϕ with respect to α: it is an explicit measure of its dependency upon α. It is worth noting that ϕ^δ exhibits the same space and time dependencies as ϕ. Definition (11) holds only for smooth flows, i.e. for flows whose solutions are differentiable with respect to α about $\alpha=\alpha_0$.

For a given control parameter α, the sensitivity equations are obtained differentiating the original Navier–Stokes system (1) with respect to α, yielding (the dependency upon x,t and α is omitted for sake of clarity)

$$\begin{aligned}
&\frac{\partial p^\delta}{\partial t}+u_i^\delta\frac{\partial p}{\partial x_i}+p^\delta\gamma\frac{\partial u_i}{\partial x_i}\\
&\quad+u_i\frac{\partial p^\delta}{\partial x_i}+p\gamma\frac{\partial u_i^\delta}{\partial x_i}-\frac{p^\delta}{C_v}\left(\frac{\partial s}{\partial t}+u_i\frac{\partial s}{\partial x_i}\right)-\frac{p}{C_v}\left(\frac{\partial s^\delta}{\partial t}+u_i^\delta\frac{\partial s}{\partial x_i}+u_i\frac{\partial s^\delta}{\partial x_i}\right)=0\\
&\rho^\delta\left(\frac{\partial u_i}{\partial t}+u_j\frac{\partial u_i}{\partial x_j}\right)+\rho\left(\frac{\partial u_i^\delta}{\partial t}+u_j^\delta\frac{\partial u_i}{\partial x_j}+u_j\frac{\partial u_i^\delta}{\partial x_j}\right)+\frac{\partial p^\delta}{\partial x_i}-\frac{\partial\tau_{ij}^\delta}{\partial x_j}=0\\
&\frac{\partial s^\delta}{\partial t}+u_i^\delta\frac{\partial s}{\partial x_i}+u_i\frac{\partial s^\delta}{\partial x_i}-\frac{Rp^\delta}{p^2}\left(\frac{\partial q_i}{\partial x_i}+\Phi\right)+\frac{R}{p}\left(\frac{\partial q_i^\delta}{\partial x_i}+\Phi^\delta\right)=0
\end{aligned} \tag{12}$$

with

$$\tau_{ij}^\delta=2(\mu^\delta s_{ij}+\mu s_{ij}^\delta)+(\lambda^\delta s_{kk}+\lambda s_{kk}^\delta)\delta_{ij},\ s_{ij}^\delta=\frac{1}{2}\left(\frac{\partial u_i^\delta}{\partial x_j}+\frac{\partial u_j^\delta}{\partial x_i}\right) \tag{13}$$

$$p^\delta=R(\rho^\delta T+\rho T^\delta) \tag{14}$$

$$q_j^\delta=-\kappa^\delta\frac{\partial T}{\partial x_j}-\kappa\frac{\partial T^\delta}{\partial x_j} \tag{15}$$

and

$$\Phi^\delta=\tau_{ij}^\delta s_{ij}+\tau_{ij}s_{ij}^\delta \tag{16}$$

The set of equations (12) is linear with respect to the sensitivity variables. It is the most general linear perturbative model derived from the Navier–Stokes equations, and can therefore be considered as an extension of the usual linearized models for acoustics and linear stability analysis. The sensitivity variables are very powerful tools providing a deep insight into the flow dynamics and the receptivity of the flow with respect to a change in the control parameter α. An interesting point is that α can be either a physical parameter or a numerical one.

Solving the linearized equations (12) is usually carried out writing a dedicated code (e.g. [4, 5]). Such a strategy is efficient when dealing with the dynamics of perturbation around a steady mean

DOI: 10.1002/fld

flow, but it suffers severe storage drawbacks when the mean flow is unsteady. Another way to solve the sensitivity equations is to use automatic differentiation of the basic flow solver (e.g. [6]).

It is worth noting that, up to now, the sensitivity variable approach has mainly been used to analyse steady flows for aerodynamic shape optimization problem (e.g. [4, 6]). It has been applied to unsteady laminar incompressible flows only very recently [5].

3. DIRECT SENSITIVITY VARIABLES COMPUTATION *VIA* COMPLEX DIFFERENTIATION

3.1. General

Here we recall the concept of complex differentiation, which was first introduced by Lyness and Moler [7]. The main advantage of complex differentiation is that in evaluating first-order derivatives, roundoff errors can be eliminated. Recall that for evaluating first derivatives of a function $f(x)$ at the point x_0, formulas like

$$f'(x_0) \approx \frac{f(x_0+\varepsilon) - f(x_0-\varepsilon)}{2\varepsilon} \tag{17}$$

are used. We are faced usually with the dilemma of using a small ε to minimize the truncation error *versus* avoiding a small ε because of computer roundoff errors, which occur when we evaluate the difference at the numerator.

In Equation (17), we replace ε with $\mathrm{i}\varepsilon$, where $\mathrm{i}^2 = -1$. To understand the approximation that we are going to make, let f be an analytic function of the complex variable z, and we assume in addition that f is real on the real axis. f may be expanded in a Taylor series about the real point x_0 as follows:

$$f(x_0 + \mathrm{i}\varepsilon) = f(x_0) + \mathrm{i}\varepsilon f'(x_0) - \frac{\varepsilon^2}{2!} f''(x_0) - \mathrm{i}\frac{\varepsilon^3}{3!} f'''(x_0) + O(\varepsilon^4) \tag{18}$$

Taking the imaginary parts of both sides of the equation and dividing both sides by ε yields

$$\frac{\mathrm{Im}[f(x_0 + \mathrm{i}\varepsilon)]}{\varepsilon} = f'(x_0) - \frac{\varepsilon^2}{3!} f'''(x_0) + O(\varepsilon^4) = f'(x_0) + O(\varepsilon^2) \tag{19}$$

Hence we obtain an approximation to $f'(x_0)$ with a truncation error of $O(\varepsilon^2)$. However, $\mathrm{Im}[f(x_0 + \mathrm{i}\varepsilon)]/\varepsilon$ is real and importantly, is not subject to subtractive cancellation, and thus we have eliminated the problem of roundoff errors. Comparisons presented in [8, 9] show that it is more accurate than the usual finite-difference approach and as accurate as the adjoint-based approach.

3.2. Complex differentiation of the unsteady compressible Navier–Stokes equations

Despite the complex differentiation technique is not recent, it has not been widely exploited up to now. It has been applied to differentiate complicated functions of a single variable in [7, 10]. It was extended to the case of the computation of the sensitivity of the drag of an airfoil with respect to wing geometrical parameters in [8, 9]. In [8], the steady Navier–Stokes equations were considered, while in [9] only the drag computation routine was differentiated. To the knowledge of the authors, the computation of the sensitivities of the full unsteady compressible Navier–Stokes equations *via* complex differentiation has not yet been addressed.

DOI: 10.1002/fld

Now let us carry out some analysis when we render all the variables in Equation (1) complex. This is straightforwardly implemented changing all real variables into complex ones in the Navier–Stokes solver. This step can be written as (for a dummy variable ϕ)

$$\phi(x,t;\alpha) \longrightarrow \phi(x,t;\alpha) + \mathrm{i}\hat{\phi}(x,t;\alpha) = \phi(x,t;\alpha) + \mathrm{i}\varepsilon\tilde{\phi}(x,t;\alpha) \tag{20}$$

where $\hat{\phi}$, $\tilde{\phi}$ and ε are the imaginary part, the rescaled imaginary part and a scaling parameter, respectively. We note by $\tilde{p}, \tilde{u}_i, \tilde{s}, \tilde{\rho}, \tilde{\tau}_{ij}, \tilde{q}_j, \tilde{\Phi}$ the corresponding rescaled imaginary parts of the variables $p, u_i, s, \rho, \tau_{ij}, q_j, \Phi$. If no imaginary perturbation is imposed, the solution will remain strictly real and identical to the solution of the usual Navier–Stokes equations.

If we introduce a perturbation to the imaginary part of the control parameter α of the order of $\varepsilon \ll 1$, then if we equate the real and imaginary parts of the system of equations, we obtain for the real part (the dependency upon x, t and α is omitted for sake of clarity):

$$\begin{aligned}
&\frac{\partial p}{\partial t} + u_i\frac{\partial p}{\partial x_i} + p\gamma\frac{\partial u_i}{\partial x_i} - \frac{p}{C_v}\left(\frac{\partial s}{\partial t} + u_i\frac{\partial s}{\partial x_i}\right) = O(\varepsilon^2)\\
&\rho\left(\frac{\partial u_i}{\partial t} + u_j\frac{\partial u_i}{\partial x_j}\right) + \frac{\partial p}{\partial x_i} - \frac{\partial \tau_{ij}}{\partial x_j} = O(\varepsilon^2)\\
&\frac{\partial s}{\partial t} + u_i\frac{\partial s}{\partial x_i} + \frac{R}{p}\left(\frac{\partial q_i}{\partial x_i} + \Phi\right) = O(\varepsilon^2)
\end{aligned} \tag{21}$$

If we equate the imaginary parts we obtain likewise:

$$\begin{aligned}
&\frac{\partial \tilde{p}}{\partial t} + \tilde{u}_i\frac{\partial p}{\partial x_i} + u_i\frac{\partial \tilde{p}}{\partial x_i}\\
&\quad + \tilde{p}\gamma\frac{\partial u_i}{\partial x_i} + p\gamma\frac{\partial \tilde{u}_i}{\partial x_i} - \frac{\tilde{p}}{C_v}\left(\frac{\partial s}{\partial t} + u_i\frac{\partial s}{\partial x_i}\right) - \frac{p}{C_v}\left(\frac{\partial \tilde{s}}{\partial t} + \tilde{u}_i\frac{\partial s}{\partial x_i} + u_i\frac{\partial \tilde{s}}{\partial x_i}\right) = O(\varepsilon^2)\\
&\tilde{\rho}\left(\frac{\partial u_i}{\partial t} + u_j\frac{\partial u_i}{\partial x_j}\right) + \rho\left(\frac{\partial \tilde{u}_i}{\partial t} + \tilde{u}_j\frac{\partial u_i}{\partial x_j} + u_j\frac{\partial \tilde{u}_i}{\partial x_j}\right) + \frac{\partial \tilde{p}}{\partial x_i} - \frac{\partial \tilde{\tau}_{ij}}{\partial x_j} = O(\varepsilon^2)\\
&\frac{\partial \tilde{s}}{\partial t} + \tilde{u}_i\frac{\partial s}{\partial x_i} + u_i\frac{\partial \tilde{s}}{\partial x_i} - \frac{R\tilde{p}}{p^2}\left(\frac{\partial q_i}{\partial x_i} + \Phi\right) + \frac{R}{p}\left(\frac{\partial \tilde{q}_i}{\partial x_i} + \tilde{\Phi}\right) = O(\varepsilon^2)
\end{aligned} \tag{22}$$

Comparing Equations (1), (12), (21) and (22), one can see that the real and imaginary parts of the complex Navier–Stokes equations are $O(\varepsilon^2)$ approximations of the original solution and its sensitivities, respectively. As a consequence, the straightforward modification of the original Navier–Stokes solver consisting as defining all arrays as complex in place of real ones makes possible to compute both the solution and its sensitivities in a single run.

Therefore, a simple way to compute the sensitivity of the Navier–Stokes solution with respect to a real computational parameter α_0 is to change it into $\alpha_0 + \mathrm{i}\varepsilon\tilde{\alpha}$. The instantaneous sensitivity variables are directly recovered from the computed imaginary part of the solution of the complex

DOI: 10.1002/fld

Navier–Stokes equations:

$$\phi^{\delta}(x,t;\alpha_0)=\frac{\hat{\phi}(x,t;\alpha_0)}{\varepsilon}+O(\varepsilon^2),\quad \phi=u_i(i=1,2,3),s,p,\rho,T \tag{23}$$

Several practical examples are given in the following.

4. BOUNDARY CONDITIONS

A very interesting feature of the pseudo-characteristic formulation is that it enables a very accurate and simple implementation of the boundary conditions. The very reason why is that using this formulation the full Navier–Stokes equations are solved at boundary nodes, fluxes associated with incoming waves being prescribed in an adequate way to enforce the targeted physical effects. Since the full equations are solved at the boundary, and not replaced by simplified surrogate models, the pseudo-characteristic formulation is expected to have a greater potential than other formulations which rely on the implementation of approximate boundary conditions.

We will explicit the real and imaginary parts of the boundary conditions in this section. The real parts of the boundary conditions are those found in Lu and Sagaut [11], with the exception that there is an extra term of the order of ε^2 in this work.

4.1. Subsonic/supersonic outflow boundary conditions

The supersonic outflow boundary condition requires no special treatment.

The definition of subsonic non-reflecting boundary conditions is straightforward. Assuming that the outflow boundary is located at the node $i=Nx$, a non-reflecting boundary condition is obtained solving the Navier–Stokes equations while setting the incoming acoustic disturbance to zero (i.e. taking $X^{-}=0$).

This is equivalent to for the real part

$$(u-c)\left(\frac{1}{\rho c}\frac{\partial p}{\partial x}-\frac{\partial u}{\partial x}\right)+O(\varepsilon^2)=0 \tag{24}$$

and the imaginary part

$$(\tilde{u}-\tilde{c})\left(\frac{1}{\rho c}\frac{\partial p}{\partial x}-\frac{\partial u}{\partial x}\right)+(u-c)\left(-\frac{\tilde{\rho}c+\rho\tilde{c}}{(\rho c)^2}\frac{\partial p}{\partial x}+\frac{1}{\rho c}\frac{\partial \tilde{p}}{\partial x}-\frac{\partial \tilde{u}}{\partial x}\right)+O(\varepsilon^2)=0 \tag{25}$$

4.2. Subsonic/supersonic inflow boundary conditions

The supersonic inflow condition is also immediately implemented, since it consists in prescribing the variation of all unknowns at the boundary nodes. This is equivalent to imposing $\partial p/\partial t$, $\partial u/\partial t$, $\partial v/\partial t$, $\partial w/\partial t$ and $\partial s/\partial t$ at each time step or to solve the Navier–Stokes equations. For a supersonic inlet, since the acoustic waves are not able to go back up the flow, we can prescribe the quantities $\partial p/\partial t$, $\partial u/\partial t$, $\partial v/\partial t$, and $\partial s/\partial t$ on the boundary for a two-dimensional case.

These four quantities allows to solve the equations on the domain boundaries by prescribing the fluxes associated with incoming characteristics. For an inlet on the left of the computational

DOI: 10.1002/fld

domain, we have for the real part

$$\begin{aligned}
X^s &= -Y^s + \frac{R}{p}\left(-\frac{\partial q_i}{\partial x_i} + \Phi\right) - \frac{\partial s}{\partial t} + O(\varepsilon^2) \\
X^v &= -\frac{1}{2}(Y^+ - Y^-) + \frac{1}{\rho}\frac{\partial \tau_{2j}}{\partial x_j} - \frac{\partial v}{\partial t} O(\varepsilon^2) \\
X^+ &= -\left(\frac{Y^+ + Y^- + 2Y^u}{2}\right) + \frac{\gamma - 1}{\rho c}\left(-\frac{\partial q_i}{\partial x_i} + \Phi\right) + \frac{1}{\rho}\frac{\partial \tau_{1j}}{\partial x_j} - \frac{1}{\rho c}\frac{\partial p}{\partial t} - \frac{\partial u}{\partial t} + O(\varepsilon^2) \\
X^- &= \left(\frac{2Y^u - Y^+ - Y^-}{2}\right) + \frac{\gamma - 1}{\rho c}\left(-\frac{\partial q_i}{\partial x_i} + \Phi\right) - \frac{1}{\rho}\frac{\partial \tau_{1j}}{\partial x_j} - \frac{1}{\rho c}\frac{\partial p}{\partial t} + \frac{\partial u}{\partial t} + O(\varepsilon^2)
\end{aligned} \tag{26}$$

where the following notations are used:

$$X^{\pm} = (u \pm c)\left(\frac{1}{\rho c}\frac{\partial p}{\partial x} \pm \frac{\partial u}{\partial x}\right) \tag{27}$$

$$X^v = u\frac{\partial v}{\partial x}, \quad X^w = u\frac{\partial w}{\partial x}, \quad X^s = u\frac{\partial s}{\partial x} \tag{28}$$

$$Y^{\pm} = (v \pm c)\left(\frac{1}{\rho c}\frac{\partial p}{\partial y} \pm \frac{\partial v}{\partial y}\right) \tag{29}$$

$$Y^u = v\frac{\partial u}{\partial y}, \quad Y^w = v\frac{\partial w}{\partial y}, \quad Y^s = v\frac{\partial s}{\partial y} \tag{30}$$

$$Z^{\pm} = (w \pm c)\left(\frac{1}{\rho c}\frac{\partial p}{\partial z} \pm \frac{\partial w}{\partial z}\right) \tag{31}$$

$$Z^u = w\frac{\partial u}{\partial z}, \quad Z^v = w\frac{\partial v}{\partial z}, \quad Z^s = w\frac{\partial s}{\partial z} \tag{32}$$

For the imaginary part, we have

$$\tilde{X^s} = -\tilde{Y^s} - \frac{R\tilde{p}}{p^2}\left(-\frac{\partial q_i}{\partial x_i} + \Phi\right) + \frac{R}{p}\left(-\frac{\partial \tilde{q_i}}{\partial x_i} + \tilde{\Phi}\right) - \frac{\partial \tilde{s}}{\partial t} + O(\varepsilon^2) \tag{33}$$

$$\tilde{X^v} = -\frac{1}{2}(\tilde{Y^+} - \tilde{Y^-}) - \frac{\tilde{\rho}}{\rho^2}\frac{\partial \tau_{2j}}{\partial x_j} + \frac{1}{\rho}\frac{\partial \tilde{\tau_{2j}}}{\partial x_j} - \frac{\partial \tilde{v}}{\partial t} + O(\varepsilon^2) \tag{34}$$

$$\begin{aligned}
\tilde{X^+} = &-\left(\frac{\tilde{Y^+} + \tilde{Y^-} + 2\tilde{Y^u}}{2}\right) - \frac{(\gamma - 1)(\rho\tilde{c} + \tilde{\rho}c)}{(\rho c)^2}\left(-\frac{\partial q_i}{\partial x_i} + \Phi\right) + \frac{\gamma - 1}{\rho c}\left(-\frac{\partial \tilde{q_i}}{\partial x_i} + \tilde{\Phi}\right) \\
&-\frac{\tilde{\rho}}{\rho^2}\frac{\partial \tau_{1j}}{\partial x_j} + \frac{1}{\rho}\frac{\partial \tilde{\tau_{1j}}}{\partial x_j} + \frac{\tilde{\rho}c + \rho\tilde{c}}{(\rho c)^2}\frac{\partial p}{\partial t} - \frac{1}{\rho c}\frac{\partial \tilde{p}}{\partial t} - \frac{\partial \tilde{u}}{\partial t} + O(\varepsilon^2)
\end{aligned} \tag{35}$$

DOI: 10.1002/fld

$$\tilde{X^-} = \left(\frac{-\tilde{Y^+} - \tilde{Y^-} + 2\tilde{Y^u}}{2}\right) - \frac{(\gamma-1)(\rho\tilde{c}+\tilde{\rho}c)}{(\rho c)^2}\left(-\frac{\partial q_i}{\partial x_i} + \Phi\right) + \frac{\gamma-1}{\rho c}\left(-\frac{\partial \tilde{q_i}}{\partial x_i} + \tilde{\Phi}\right)$$
$$+\frac{\tilde{\rho}}{\rho^2}\frac{\partial \tau_{1j}}{\partial x_j} - \frac{1}{\rho}\frac{\partial \tilde{\tau_1}_j}{\partial x_j} + \frac{\tilde{\rho}c+\rho\tilde{c}}{(\rho c)^2}\frac{\partial p}{\partial t} - \frac{1}{\rho c}\frac{\partial \tilde{p}}{\partial t} - \frac{\partial \tilde{u}}{\partial t} + O(\varepsilon^2) \tag{36}$$

The pseudo-characteristic formulation also enables the definition of fully consistent exact inflow conditions in the subsonic case. Considering the case of a subsonic inflow condition at the boundary $i = 1$, one can see that the definition of such a condition is equivalent to prescribing X^+, X^s, X^v and X^w at this location at each time step. Since there are four unknown fluxes and five unknown physical variables, one recovers the well-known results that the time variation of all physical unknowns cannot be prescribed at the same time.

A careful examination of the system of governing equations shows that prescribing $\partial v/\partial t$ and $\partial w/\partial t$ is equivalent to prescribing values for X^v and X^w. To obtain a well-posed problem, one condition must be prescribed for each of these two velocity components. The three remaining physical variables (namely p, u and s) being coupled at the interface, they cannot be treated separately. A consistent inflow condition will therefore consist in finding values of $\partial p/\partial t$, $\partial s/\partial t$ and $\partial u/\partial t$ (or in an equivalent manner X^+ and X^s) at the inlet plane. A large number of combinations can be defined, depending on the prescribed quantities.

If $\partial u/\partial t$ and $\partial s/\partial t$ are prescribed, then we obtain for the real part

$$\begin{aligned}
X^+ &= X^- + 2Y^u + \frac{2}{\rho}\frac{\partial \tau_{1j}}{\partial x_j} - 2\frac{\partial u}{\partial t} + O(\varepsilon^2)\\
X^v &= -\left(\frac{\partial v}{\partial t} + \frac{1}{2}(Y^+ - Y^-)\right) + \frac{1}{\rho}\frac{\partial \tau_{2j}}{\partial x_j} + O(\varepsilon^2)\\
X^s &= -Y^s - \frac{\partial s}{\partial t} + \frac{R}{p}\left(-\frac{\partial q_i}{\partial x_i} + \Phi\right) + O(\varepsilon^2)
\end{aligned} \tag{37}$$

For the imaginary part, we have

$$\begin{aligned}
\tilde{X^+} &= \tilde{X^-} + 2\tilde{Y^u} - \frac{2\tilde{\rho}}{\rho^2}\frac{\partial \tau_{1j}}{\partial x_j} + \frac{2}{\rho}\frac{\partial \tilde{\tau_1}_j}{\partial x_j} - 2\frac{\partial \tilde{u}}{\partial t} + O(\varepsilon^2)\\
\tilde{X^v} &= -\left(\frac{\partial \tilde{v}}{\partial t} + \frac{1}{2}(\tilde{Y^+} - \tilde{Y^-})\right) - \frac{\tilde{\rho}}{\rho^2}\frac{\partial \tau_{2j}}{\partial x_j} + \frac{1}{\rho}\frac{\partial \tilde{\tau_2}_j}{\partial x_j} + O(\varepsilon^2)\\
\tilde{X^s} &= -\tilde{Y^s} - \frac{\partial \tilde{s}}{\partial t} - \frac{R\tilde{p}}{p^2}\left(-\frac{\partial q_i}{\partial x_i} + \Phi\right) - \frac{R}{p}\left(-\frac{\partial \tilde{q_i}}{\partial x_i} + \tilde{\Phi}\right) + O(\varepsilon^2)
\end{aligned} \tag{38}$$

It is important to note that these boundary conditions are exact, since they are directly derived from the Navier–Stokes equations without any assumptions. Therefore, they are consistent from a thermodynamic viewpoint.

DOI: 10.1002/fld

4.3. Rigid/compliant isothermal wall

Let us address now the modelling of an infinitely rigid or moving isothermal wall. In the two-dimensional case, the boundary conditions are of the following form:

$$Y^u = -\frac{\partial u}{\partial t} - \frac{1}{2}(X^+ - X^-) + \frac{1}{\rho}\frac{\partial \tau_{1j}}{\partial x_j} + O(\varepsilon^2) \tag{39}$$

$$Y^+ = 2\left(-\frac{\partial v}{\partial t} - X^v + \frac{1}{2}Y^- + \frac{1}{\rho}\frac{\partial \tau_{2j}}{\partial x_j}\right) + O(\varepsilon^2) \tag{40}$$

$$Y^s = -X^s + \frac{R}{p}\left(-\frac{\rho c}{2}(X^+ + X^- + Y^+ + Y^-) + \gamma\left(-\frac{\partial q_i}{\partial x_i} + \Phi\right)\right) + O(\varepsilon^2) \tag{41}$$

The imaginary part is the following:

$$\tilde{Y^u} = -\frac{\partial \tilde{u}}{\partial t} - \frac{1}{2}(\tilde{X^+} - \tilde{X^-}) - \frac{\tilde{\rho}}{\rho^2}\frac{\partial \tau_{1j}}{\partial x_j} + \frac{1}{\rho}\frac{\partial \tilde{\tau_{1j}}}{\partial x_j} + O(\varepsilon^2) \tag{42}$$

$$\tilde{Y^+} = 2\left(-\frac{\partial \tilde{v}}{\partial t} - \tilde{X^v} + \frac{1}{2}\tilde{Y^-} - \frac{\tilde{\rho}}{\rho^2}\frac{\partial \tau_{2j}}{\partial x_j} + \frac{1}{\rho}\frac{\partial \tilde{\tau_{2j}}}{\partial x_j}\right) + O(\varepsilon^2) \tag{43}$$

$$\begin{aligned}\tilde{Y^s} = -X^s - \frac{R\tilde{p}}{p^2}\left(-\frac{\rho c}{2}(X^+ + X^- + Y^+ + Y^-) + \gamma\left(-\frac{\partial q_i}{\partial x_i} + \Phi\right)\right) + \frac{\gamma R}{p}\left(-\frac{\partial \tilde{q_i}}{\partial x_i} + \tilde{\Phi}\right)\\ + \frac{R}{p}\left(-\frac{(\tilde{\rho}c - \rho\tilde{c})}{2}(X^+ + X^- + Y^+ + Y^-) - -\frac{\rho c}{2}(\tilde{X^+} + \tilde{X^-} + \tilde{Y^+} + \tilde{Y^-})\right)\end{aligned} \tag{44}$$

The rigid wall boundary condition is recovered taking $\partial u/\partial t = \partial v/\partial t = 0$. The same system of equation can be used to model a porous boundary with a prescribed transpiration velocity. An important point is that, once again, the boundary condition is exact and fully consistent from a thermodynamic viewpoint.

5. BRIEF PRESENTATION OF THE NUMERICAL METHOD

The numerical method utilized in the present study is the same as the one described in [11]. Since the complex differentiation strategy does not rely on any assumption on the flow solver, it will not be detailed here. Only its main elements will be recalled below. The interested reader can refer to the original publication for an exhaustive description of the numerical method. It is based on the pseudo-characteristic formulation of the convection terms introduced by Sesterhenn [12] and further developed by Lu and Sagaut [11].

This new decomposition of the pressure, velocity and entropy fluxes enables a very simple and natural use of upwind schemes to enforce numerical stability while minimizing the numerical dissipation.

In the present work, all inviscid fluxes are written in a quasi-linear form and appear under the generic form $(u(\partial\phi/\partial x))$, where u is the advecting velocity and ϕ the advected quantity. To

DOI: 10.1002/fld

enforce both numerical stability and accuracy for wave propagation problems, it is chosen here to use high-order upwind Dispersion Relation Preserving schemes for all fluxes.

At interior nodes (i.e. for grid point with index $5 \leqslant i \leqslant Nx-2$, where Nx is the index of the last grid point) the following fourth-order accurate upwind biased Dispersion Relation Preserving scheme is used:

$$\left(u\frac{\partial\phi}{\partial x}\right)_i = u_i \frac{1}{\Delta x}\sum_{k=-4,2} a_k \phi_{i+k} \tag{45}$$

with

$$a_{-4}=0.0161404967151, \quad a_{-3}=-0.122821279020, \quad a_{-2}=0.455332277706$$

$$a_{-1}=-1.2492595882615, \quad a_0=0.5018904380193, \quad a_1=0.4399321927296$$

$$a_2=-0.04121453788895$$

where it was assumed that the convection speed u is positive. The above DRP scheme is modified as follows near the computational domain boundaries:

- at $i=Nx$, a sixth-order one-sided upwind scheme is utilized:

$$\left(u\frac{\partial\phi}{\partial x}\right)_i = u_i \frac{1}{\Delta x}\sum_{k=-6,0} a_k \phi_{i+k}$$
$$a_{-6}=1/60, \quad a_{-5}=-6/5, \quad a_{-4}=15/4, \quad a_{-3}=20/3 \tag{46}$$
$$a_{-2}=15/2, \quad a_{-1}=-6, \quad a_0=49/20$$

- at $i=Nx-1$, the following upwind-biased DRP scheme proposed in [13] is implemented

$$\left(u\frac{\partial\phi}{\partial x}\right)_i = u_i \frac{1}{\Delta x}\sum_{k=-5,1} a_k \phi_{i+k}$$
$$a_{-5}=-0.0306489732244242, \quad a_{-4}=0.202225858313369$$
$$a_{-3}=-0.634728026533812, \quad a_{-2}=1.29629965415671 \tag{47}$$
$$a_{-1}=-2.14305478803459, \quad a_0=1.10888726751399$$
$$a_1=0.201019007808754$$

- at $i=4$, a fifth-order upwind-biased scheme is used:

$$\left(u\frac{\partial\phi}{\partial x}\right)_i = u_i \frac{1}{\Delta x}\sum_{k=-3,2} a_k \phi_{i+k} \tag{48}$$
$$a_{-3}=-1/30, \quad a_{-2}=1/4, \quad a_{-1}=-1, \quad a_0=1/3, \quad a_1=1/2, \quad a_2=-1/20$$

DOI: 10.1002/fld

- at $i=3$, it is replaced by the following third-order upwind scheme

$$\left(u\frac{\partial\phi}{\partial x}\right)_i = u_i\frac{1}{\Delta x}\sum_{k=-2,1} a_k\phi_{i+k}$$
$$a_{-2}=1/6, \quad a_{-1}=-1, \quad a_0=1/2, \quad a_1=1/3 \tag{49}$$

- at $i=2$, the first-order upwind scheme is used

$$\left(u\frac{\partial\phi}{\partial x}\right)_i = u_i\frac{1}{\Delta x}\sum_{k=-1,0} a_k\phi_{i+k}$$
$$a_{-1}=-1, \quad a_0=1 \tag{50}$$

- at $i=1$, the following downwind scheme is used:

$$\left(u\frac{\partial\phi}{\partial x}\right)_i = u_i\frac{1}{\Delta x}\sum_{k=0,2} a_k\phi_{i+k}$$
$$a_0=-3/5, \quad a_1=4/5, \quad a_2=-1/5 \tag{51}$$

The time integration is performed using the third-order TVD Runge–Kutta scheme proposed by Shu and Osher [14]:

$$\begin{aligned} u^{n,1} &= u^n + \Delta t\left(\frac{\partial u^n}{\partial t}\right) \\ u^{n,2} &= \frac{1}{4}\left(3u^n + u^{n,1} + \Delta t\left(\frac{\partial u^{n,1}}{\partial t}\right)\right) \\ u^{n+1} &= \frac{1}{3}\left(u^n + 2u^{n,2} + 2\Delta t\left(\frac{\partial u^{n,2}}{\partial t}\right)\right) \end{aligned} \tag{52}$$

6. NUMERICAL SIMULATIONS

We now illustrate the potential of the proposed method considering simple but meaningful test cases. The issue of sensitivity of a smooth compressible flow is formally close to the problem of its linear instability properties: a linearly stable flow is expected to weakly respond to a perturbation, i.e. to have weak sensitivity variables, while an instable flow will exhibit large sensitivities. The sensitivity variables can also be used to gain an insight into possible couplings between the physical modes defined by Kovasznay (namely: vorticity mode, entropy mode and acoustic mode) [15].

6.1. Sensitivity of a two-dimensional inviscid acoustic wave

We consider the evolution of an initial two-dimensional acoustic pulse in a fluid at rest. The computational domain is $[0,40]^2$ and outflow conditions are applied on all boundaries of the computational domain. The mesh is uniform with $\Delta x=\Delta y=0.2$.

DOI: 10.1002/fld

The initial disturbance is defined as

$$\rho(x, y, t=0) = \Gamma e^{-\alpha(x^2+y^2)}(1 + i\varepsilon) \tag{53}$$

$$p(x, y, t=0) = c_0^2 \rho \quad (x, y, t=0) \tag{54}$$

$$u(x, y, t=0) = v(x, y, t=0) = 0 \tag{55}$$

with $\Gamma = 0.01$, $b = 3$, and $\varepsilon = 10^{-6}$. Here, c_0 denotes the speed of sound in the unperturbed fluid. The complex perturbation added to the initial density disturbance will lead to the computation of the sensitivity of the solution with respect to the amplitude of the initial density fluctuation. The time-step Δt is chosen such that $\mathrm{CFL} \equiv c\Delta t/\Delta x = 0.5$.

The instantaneous sensitivity of the pressure field at $250\Delta t$ is displayed in Figure 1 for different values of the control parameter ε. First, one can see that the sensitivity fields obtained for the different values of ε are identical, showing that the solution is converged with respect to this parameter. This robustness with respect to the parameter ε was observed in previous studies dealing with the differentiation of scalar function or the incomplete gradient computation [9]. It is shown here that it is also true when computing the instantaneous sensitivities of the full compressible Navier–Stokes equations.

It is observed that the sensitivity of the pressure is associated with the isotropic acoustic wave which is emitted at the initial time due to the relaxation of the initial perturbation, leading to the occurence of an acoustic sensitivity wave, whose wavelength is identical to the one of the physical wave. Therefore, one can deduce that the amplitude of radiated acoustic field acoustic field can be modified changing the amplitude of the initial density disturbance. This conclusion is in perfect agreement with the linear acoustic theory.

We now investigate the sensitivity of the inviscid acoustic wave with respect to an entropy disturbance. To this end, instead of perturbing ρ, we perturb the entropy of the system by $\varepsilon = 10^{-6}$. The instantaneous sensitivity of the pressure field at $250\Delta t$ is shown in Figure 2. As in the previous case, one can observe that the occurence of a sensitivity wave of acoustic nature. It is interesting to note that while the acoustic waves are essentially an isentropic phenomena (at a first order of approximation), the amplitude of the emitted acoustic wave may be governed by a change in the initial entropy field. This fact may be understood in looking at the governing equations for the sensitivity variables: it is seen that p^δ has a direct dependency upon s and s^δ.

6.2. Sensitivity of a vortex in a supersonic flow

We now illustrate the proposed method to study the sensitivity of a vortex advected by a supersonic uniform flow.

At $t = 0$, we introduce at the centre of the computational domain, a two-dimensional vortex with the following initial conditions:

$$u(x, y) = u_0 + a_0 y \exp[-\ln 2(x^2 + y^2)] \tag{56}$$

$$v(x, y) = -a_0 x \exp[-\ln 2(x^2 + y^2)] \tag{57}$$

where u and v are the velocity component in the x and y direction, respectively. The base flow is uniform with the Mach number u_0/c_0 equal to 3. The amplitude parameter is chosen so that $a_0/c_0 = \frac{1}{34}$, where c_0 is the speed of sound associated to the base flow. The computational domain is $[0, 20]^2$ and a uniform mesh $\Delta x = \Delta y = 0.1$ is used.

DOI: 10.1002/fld

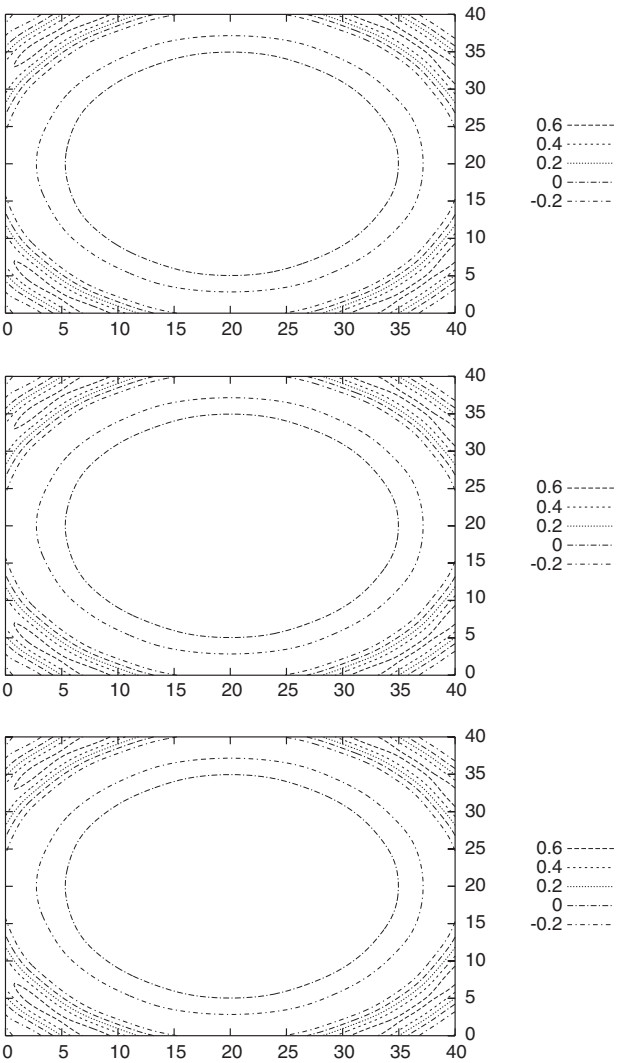

Figure 1. Instantaneous sensitivity of the pressure field due to an initial density perturbation at $t = 250\Delta t$ for different values of the control parameter. Top: $\varepsilon = 10^{-4}$; middle: $\varepsilon = 10^{-5}$; bottom: $\varepsilon = 10^{-6}$.

Let us first consider a perturbation of the pressure field in the vortex region, that is to say

$$p(x, y, t = 0) = p_0 + \mathrm{i}\varepsilon \exp[-\ln 2(x^2 + y^2)] \tag{58}$$

where $\varepsilon = 10^{-6}$ and p_0 is the uniform reference pressure. The sensitivity of the pressure field at $250\Delta t$ is presented in Figure 3. We observe the advection of the sensitivity of the pressure field, which corresponds here to the advection of the vortex. It is observed here that the pressure sensitivity is advected at the base flow speed, and therefore does not correspond to an acoustic wave but to an hydrodynamic mode.

DOI: 10.1002/fld

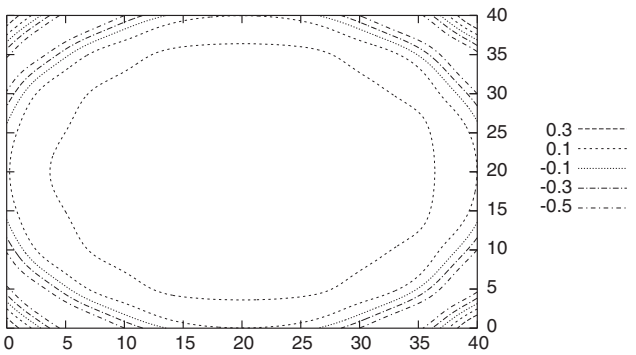

Figure 2. Instantaneous sensitivity of the pressure field due to an initial entropy perturbation at $250\Delta t$.

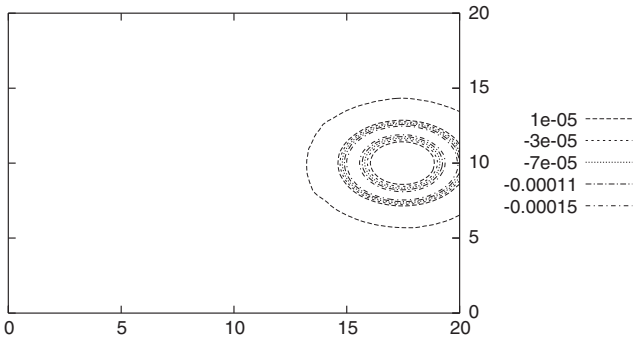

Figure 3. Vortex advected by a uniform supersonic flow. Instantaneous sensitivity of the pressure field due to an initial pressure perturbation at time $250\Delta t$.

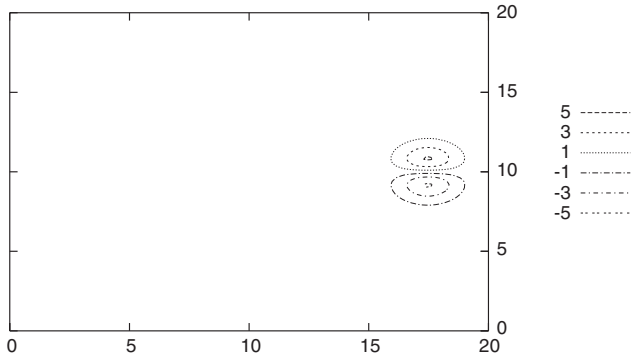

Figure 4. Vortex advected by a uniform supersonic flow. Instantaneous sensitivity of the streamwise velocity component at time $250\Delta t$ due to an initial circulation perturbation.

DOI: 10.1002/fld

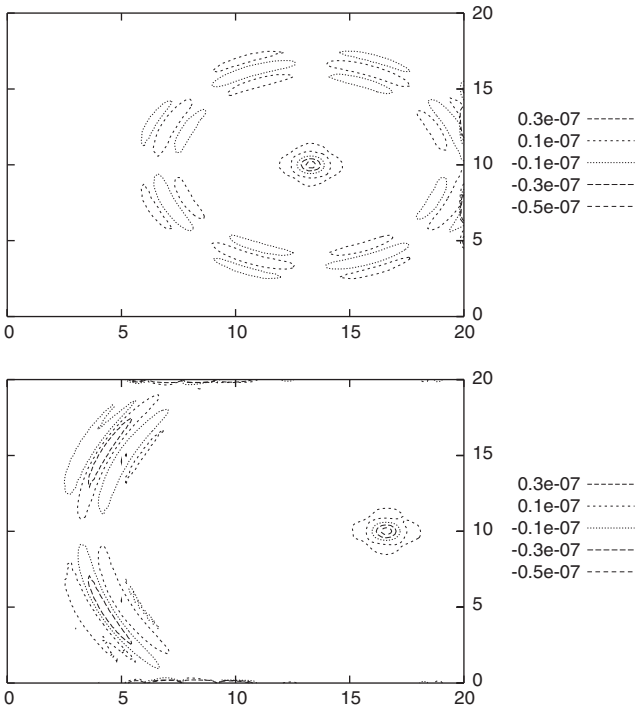

Figure 5. Vortex in a subsonic uniform flow. Instantaneous sensitivity of the vorticity field due to an initial pressure perturbation at $250\Delta t$ (top) and $500\Delta t$ (bottom).

Now let us consider an initial perturbation of the vortex initial circulation, defined as

$$u(x, y) = a_0 y \exp[-\ln 2(x^2 + y^2)](1 + \mathrm{i}\varepsilon) \tag{59}$$

$$v(x, y) = -a_0 x \exp[-\ln 2(x^2 + y^2)](1 + \mathrm{i}\varepsilon) \tag{60}$$

The sensitivity of the streamwise velocity component u at time $250\Delta t$ is presented in Figure 4. It is associated to an hydrodynamic mode, namely a vorticity sensitivity mode.

6.3. Sensitivity of a vortex in a subsonic flow

We now consider the case of a vortex advected by a subsonic base flow. The initial perturbations and the computational parameters are identical to those in the case of a supersonic flow. The only modification is the Mach number u_0/c_0 which is equal to 0.5 in this case.

Let us first consider a Gaussian perturbation of the initial pressure field in the vortex region, that is to say

$$p(x, y, t = 0) = \mathrm{i}\varepsilon \exp[-\ln 2(x^2 + y^2)] \tag{61}$$

where $\varepsilon = 10^{-6}$.

DOI: 10.1002/fld

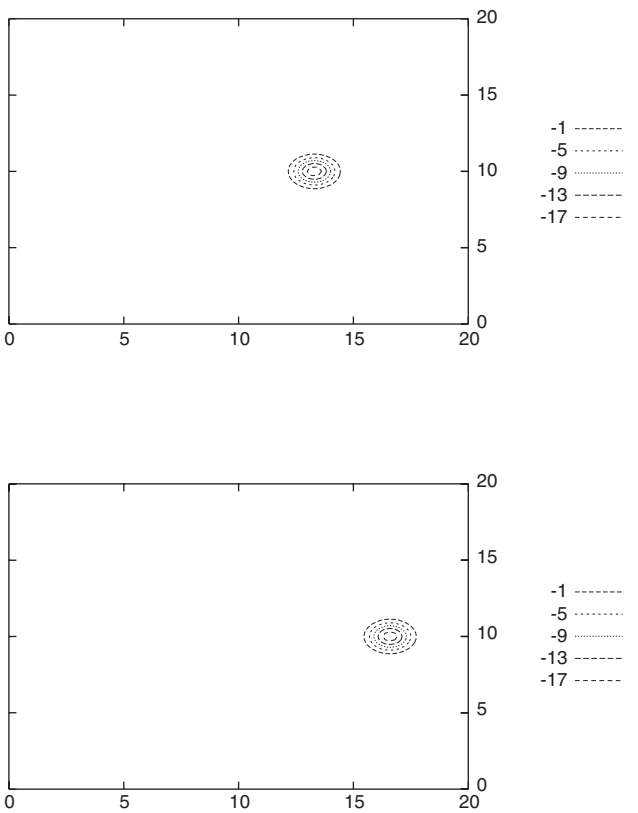

Figure 6. Vortex in a subsonic uniform flow. Instantaneous sensitivity of the vorticity field due to an initial circulation perturbation at times $250\Delta t$ (top) and $500\Delta t$ (bottom).

The sensitivity of the vorticity field $\omega = \mathrm{curl}(u)$, defined as (where, as above, α is a dummy control parameter)

$$\omega^{\delta} \equiv \frac{\partial \omega}{\partial \alpha} = \mathrm{curl}(u^{\delta}) \tag{62}$$

at times $250\Delta t$ and $500\Delta t$ is presented in Figure 5. One can see that, in the subsonic regime, the vorticity sensitivity is composed of a circular wave with azimuthal modulation that propagates with the speed of sound with respect to the base flow and an hydrodynamic mode that is advected at speed u_0. The sensitivity is weak, since the amplitude of ω^{δ} is $O(10^{-7})$. This is in agreement with the fact that vorticity, entropy and acoustic modes are decoupled at the first order of approximation in a uniform flow.

Now let us consider a perturbation of the circulation of the vortex at the initial time, defined as

$$u(x, y) = a_0 y \exp[-\ln 2(x^2 + y^2)](1 + \mathrm{i}\varepsilon) \tag{63}$$

$$v(x, y) = -a_0 x \exp[-\ln 2(x^2 + y^2)](1 + \mathrm{i}\varepsilon) \tag{64}$$

DOI: 10.1002/fld

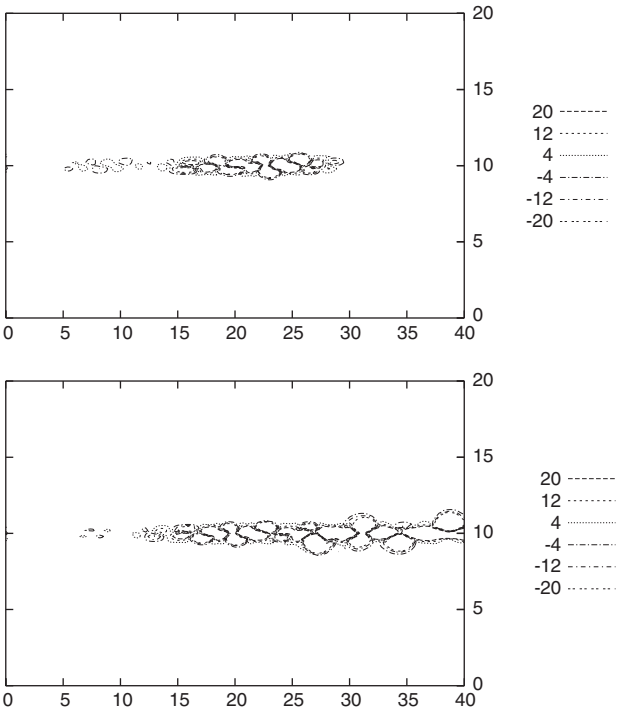

Figure 7. Mixing layer with random inlet velocity perturbation. Iso-contours of the vorticity field due to a random upstream velocity perturbation with $\Omega = 100$ at time $1000\Delta t$ (top) and $1500\Delta t$ (bottom).

The sensitivities of the vorticity field at times $250\Delta t$ and $500\Delta t$ are presented in Figure 6. It is observed that, in this case, the sensitivity has no acoustic component, and corresponds to a vorticity mode advected at speed u_0.

6.4. Sensitivity analysis of a subsonic mixing layer

As a final application, we consider a two-dimensional spatially developing mixing layer. The computational domain is $[0, 40] \times [0, 20]$ with a uniform mesh $\Delta x = \Delta y = 0.1$. The base inlet velocity has a hyperbolic tangent profile

$$u_0(y) = U + \frac{U}{2}(\tanh(5(y - 10)) + 1) \tag{65}$$

where $U = c_0/4$. Uniform base pressure and density fields are considered. The mixing layer is known to be inviscidly unstable. A perturbation leads to the generation of vortices by Kelvin–Helmholtz instability [2]. A random perturbation on the streamwise velocity component at the inlet plane is imposed to trigger unsteadiness. It is defined as

$$u(0, y, t) = \Gamma R(t) c \exp(-2(y - 10)^2) \tag{66}$$

where $R(t)$ is a random variable which takes its value between $[-1, 1]$ and $\Gamma = 0.01$.

DOI: 10.1002/fld

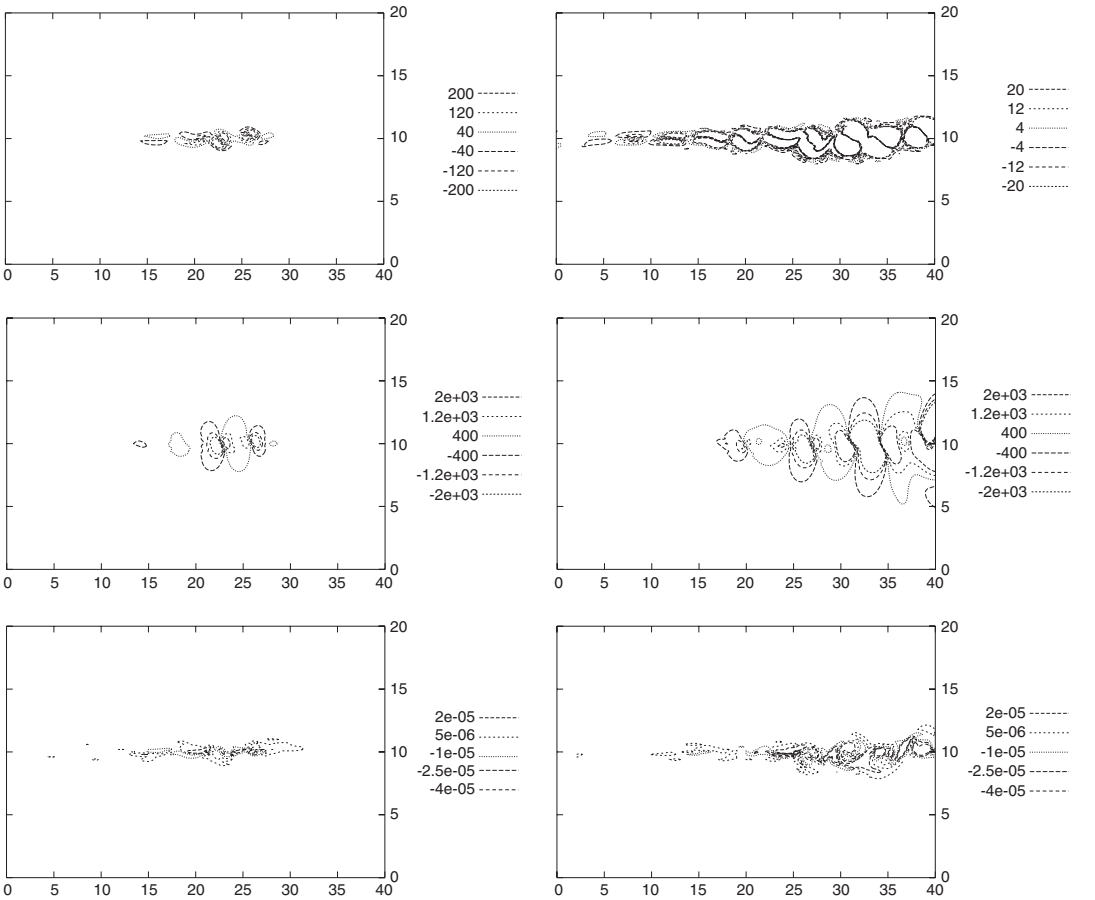

Figure 8. Mixing layer with random inlet velocity perturbation. Instantaneous sensitivity of the vorticity (top), pressure (middle) and entropy (bottom) fields due to a random upstream velocity perturbation with $\Omega = 100$ at time $1000\Delta t$ (left) and $1500\Delta t$ (right).

Let us first consider the sensitivity of the flow with respect to a coherent inlet velocity perturbation. To this end, we introduce the following imaginary part to u:

$$\hat{u}(0, y, t) = \mathrm{i}\Gamma\varepsilon c \sin(\Omega t) \exp(-2(y - 10)^2) \tag{67}$$

leading to the following complex inlet streamwise velocity perturbation:

$$u(0, y, t) = \Gamma c \exp(-2(y - 10)^2)(R(t) + \mathrm{i}\varepsilon \sin(\Omega t)) \tag{68}$$

where the frequency is taken equal to $\Omega = 100$ and $\varepsilon = 10^{-6}$. The sensitivity field will be related to the receptivity of the randomly forced mixing layer to a coherent velocity forcing with frequency Ω.

We present in Figure 7 two views of the instantaneous vorticity field, which show the formation of vortices. Due to the randomness of the inlet aerodynamic perturbation, the vortices do not form

DOI: 10.1002/fld

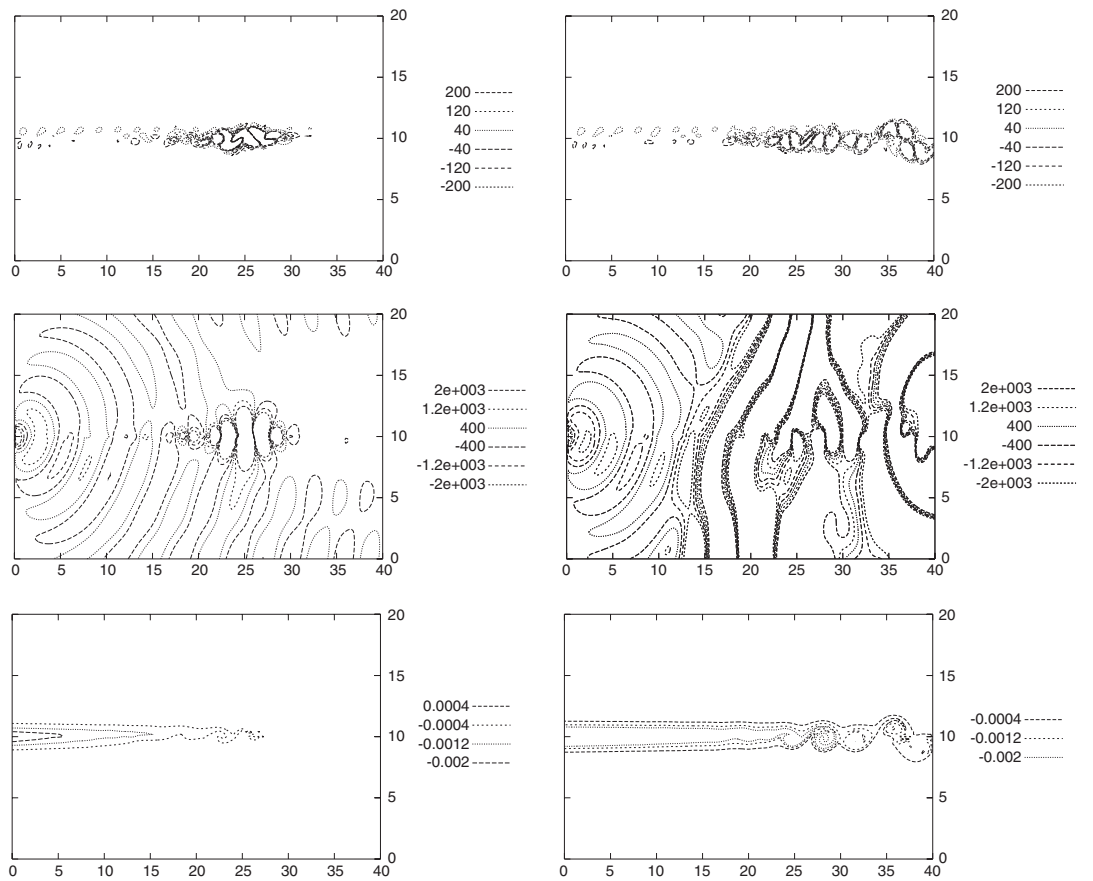

Figure 9. Mixing layer with random inlet velocity perturbation. Instantaneous sensitivity of the vorticity (top), pressure (middle) and entropy (bottom) fields due to an upstream pressure perturbation with $\Omega = 500$ at time $1000\Delta t$ (left) and $2000\Delta t$ (right).

a regular pattern. In Figure 8, the corresponding sensitivities of the solution are displayed. It is observed that the sensitivity patterns are associated with coherent vortices, meaning that these structures would be affected by the coherent velocity perturbation. The same observation holds for both the pressure and the entropy sensitivity: they are associated with hydrodynamic modes, not to acoustic-type waves. It is worth noting that the sensitivity analysis enables the determination of the response of full solution to the selected upstream disturbance, and to identify the couplings that exist between vorticity, pressure and entropy waves in flows which is out of the original Kovasznay framework.

We now investigate the sensitivity of the same base flow (Equation (65)) with the same real random velocity perturbation (Equation (66)) with respect to a coherent pressure forcing. To this end, the following imaginary pressure perturbation is imposed at the inlet plane:

$$p(0, y, t) = \hat{p}(0, y, t) = \mathrm{i}\varepsilon\Gamma p_{\mathrm{ref}} \sin(\Omega t) \exp(-2(y - 10)^2) \tag{69}$$

DOI: 10.1002/fld

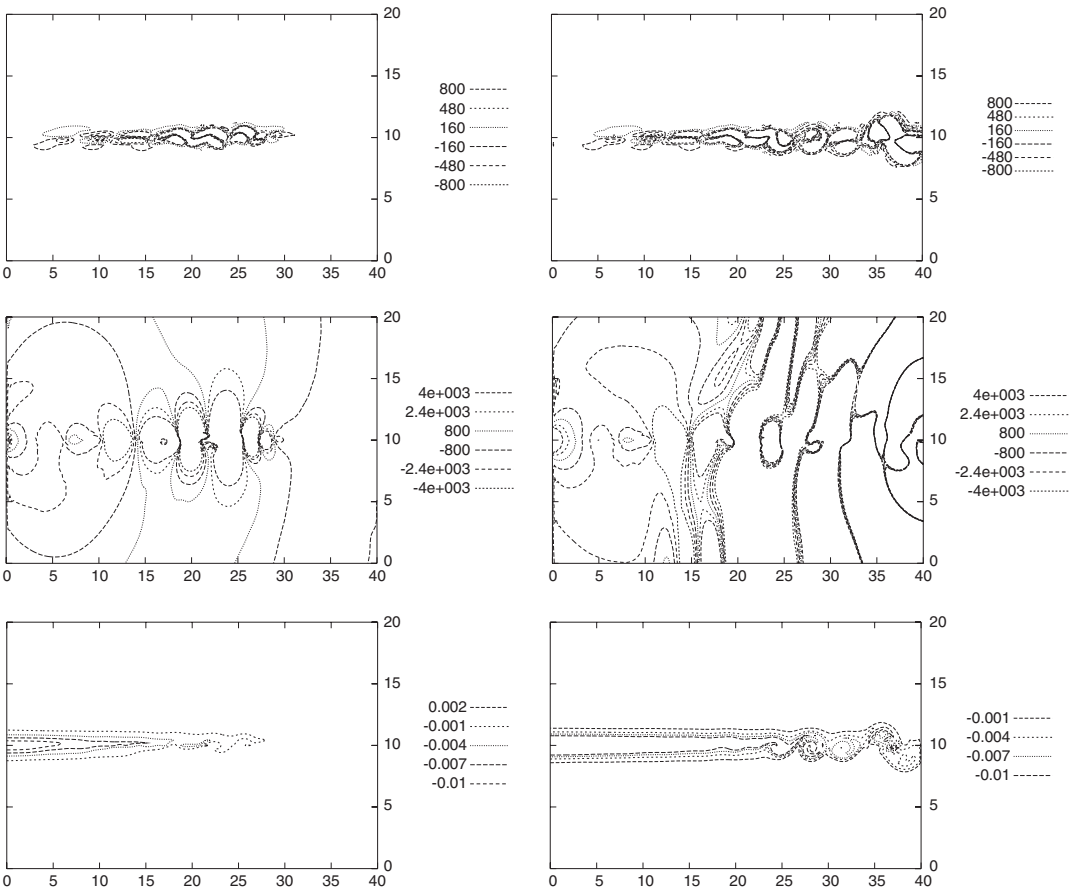

Figure 10. Mixing layer with random inlet velocity perturbation. Instantaneous sensitivity of the vorticity (top), pressure (middle) and entropy (bottom) fields due to an upstream pressure perturbation with $\Omega = 100$ at time $1000\Delta t$ (left) and $2000\Delta t$ (right).

where p_{ref} is a reference pressure level associated with the base flow, $\Gamma = 0.01$ the amplitude parameter and ε is taken equal to 10^{-6} as in previous cases. The instantaneous sensitivity fields are displayed in Figures 10 and 9, for $\Omega = 100$ and $\Omega = 500$, respectively.

We now emphasize the difference that exists between the sensitivity of an instantaneous flow and the one of the associated base flow. To this end, we consider the same base flow given by Equation (65), but we impose a real pressure disturbance at the inlet in place of the velocity disturbance considered in the previous case. To obtain a meaningful comparison, the inlet pressure perturbation is taken similar to the imaginary one used above:

$$p(0, y, t) = \gamma p_{\text{ref}} \sin(\Omega t) \exp(-2(y - 10)^2)(1 + \mathrm{i}\varepsilon) \tag{70}$$

We will consider the effects of varying Ω. The sensitivity of the solution is presented in Figure 11 for $\Omega = 500$ and in Figure 12 for $\Omega = 100$. The response of the mixing layer is observed to

DOI: 10.1002/fld

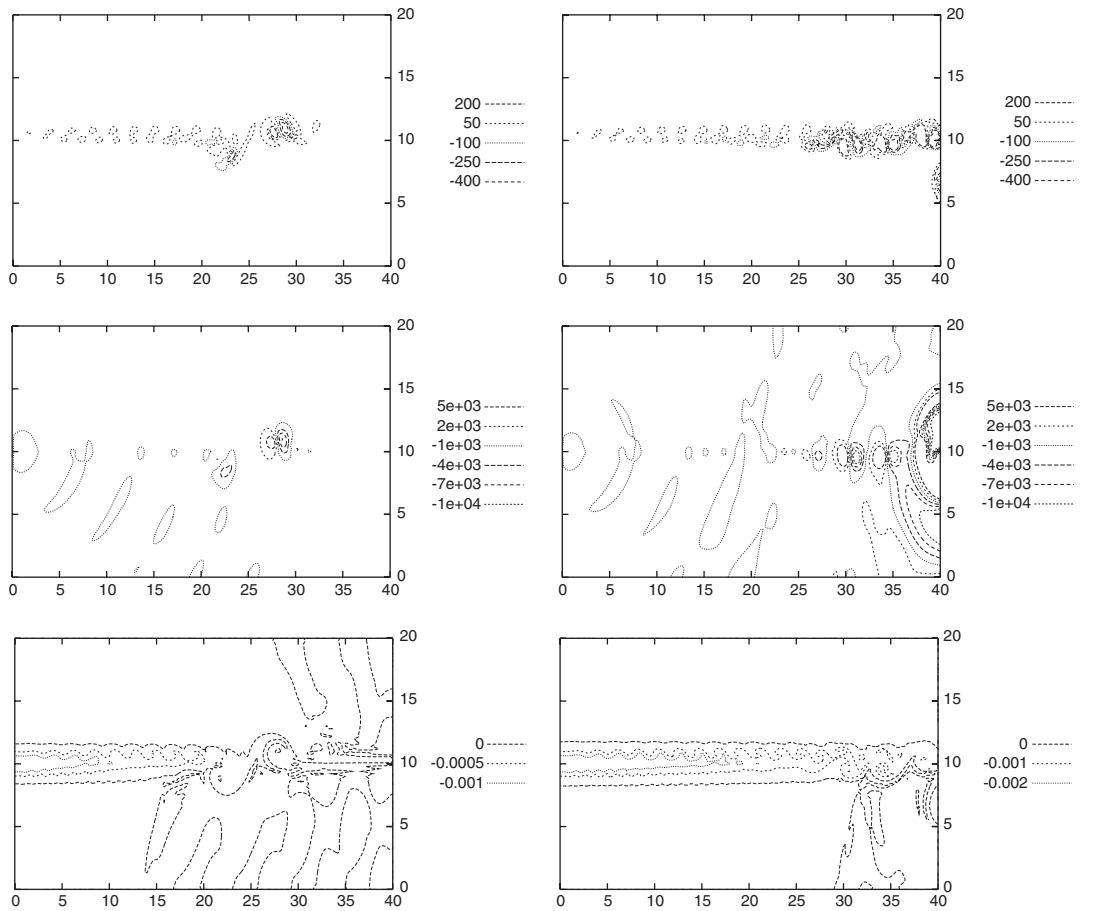

Figure 11. Mixing layer with coherent inlet pressure perturbation. Instantaneous sensitivity of the vorticity (top), pressure (middle) and entropy (bottom) fields due to an upstream pressure perturbation with $\Omega = 500$ at time $1000\Delta t$ (left) and $2000\Delta t$ (right).

be very dependent upon the forcing frequency, in agreement with known results dealing with the dynamics of free shear layer. The sensitivity patterns are mainly associated with hydrodynamic events, which are much more energetic than acoustic waves. But it is worth noting that for $\Omega = 500$, both the pressure and entropy sensitivities exhibit patterns associated to acoustic sensitivity waves outside the mixing layer region. This is in agreement with the fact that the mixing layer emits acoustic waves and that acoustic waves generate (weak) entropy disturbances in the viscous regime.

The patterns of the flow exhibit striking differences with the one obtained considering the sensitivity of the same base flow with a real random velocity perturbation. The very reason why the sensitivity is nothing but a measure of the gradient of the instantaneous solution to with respect to the control parameter (the amplitude of the pressure forcing term in the present case). The sensitivity field is therefore related to the linear response of a non-linear flow with respect to the considered parameter.

DOI: 10.1002/fld

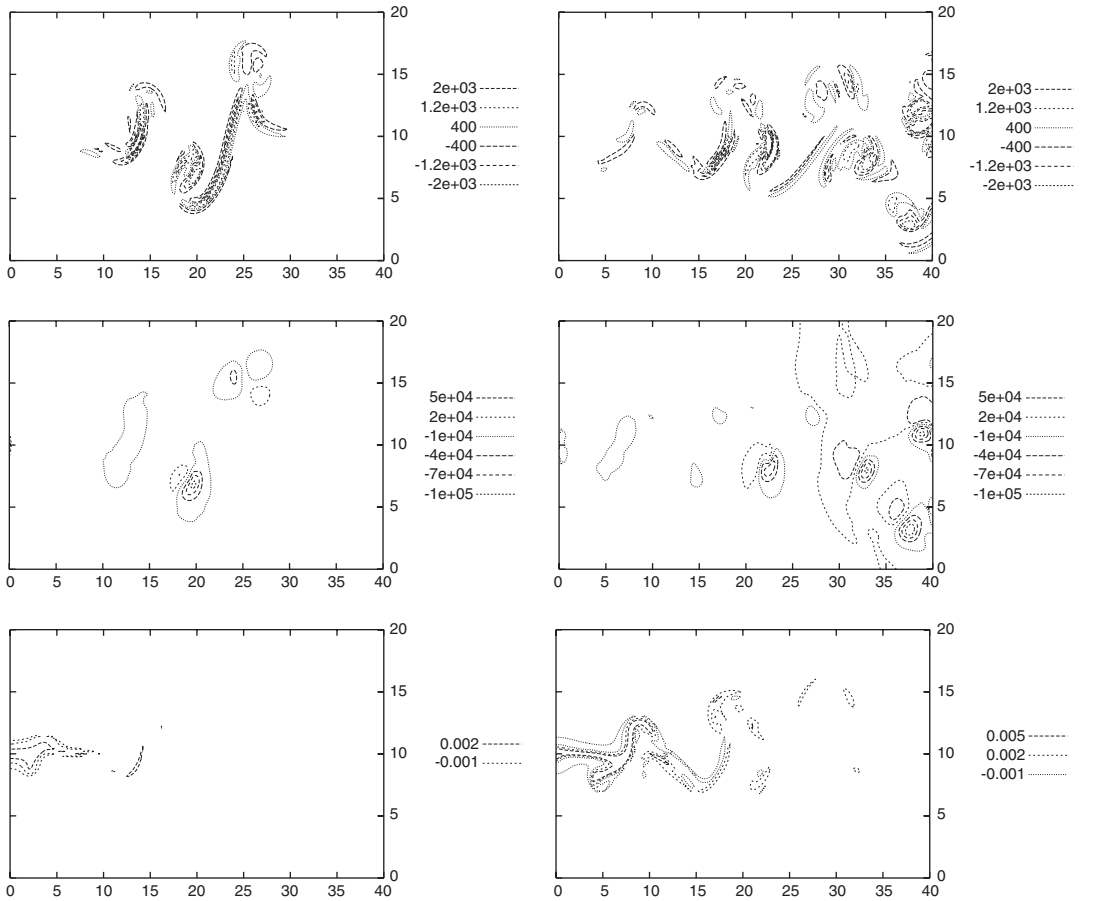

Figure 12. Mixing layer with coherent inlet pressure perturbation. Instantaneous sensitivity of the vorticity (top), pressure (middle) and entropy (bottom) fields due to an upstream pressure perturbation with $\Omega = 100$ at time $1000\Delta t$ (left) and $2000\Delta t$ (right).

7. CONCLUSION

A method which makes possible to compute both the flow and its sensitivities with respect to a parameter in a single run thanks to a simple modification of the original Navier–Stokes solver has been presented and assessed on several examples of practical relevance. The method was observed to be robust with respect to the control parameter ε and to yield useful $O(\varepsilon^2)$ approximation of the exact sensitivities.

The method is well suited to compute instantaneous sensitivities of unsteady flows, and does not rely on any assumptions on the base flow, the geometry and the Navier–Stokes solver. It is therefore a fully general method, that can be employed on flows with complex geometries.

It was observed that the instantaneous sensitivity fields can be interpreted, thanks to Kovasznay decomposition as the combination of waves of several types (namely: acoustic, vorticity and entropy waves).

DOI: 10.1002/fld

The present approach can be used to compute flow gradient with respect to control or shape optimization parameter, but also to extend the notion of acoustic/hydrodynamic sources. The latter point is presently under investigation by the authors.

REFERENCES

1. Walters RW, Huyse L. Uncertainty analysis for fluid mechanics with applications. *ICASE Technical Report 2002-1*, 2002.
2. Huerre P, Rossi M. Hydrodynamic instabilities in open flows. In *Hydrodynamics and Nonlinear Instabilities*, Godreche C, Manneville P (eds). Cambridge University Press: Cambridge, MA, 1998; 81–294.
3. Schmid PJ, Henningson DS. *Stability and Transition in Shear Flows*. Springer: New York, 2001.
4. Borggaard J, Burns J. A PDE sensitivity equation method for optimal aerodynamic design. *Journal of Computational Physics* 1997; **136**:366–384.
5. Hristova H, Etienne S, Pelletier D, Borggaard J. A continuous sensitivity equation method for time dependent incompressible laminar flows. *International Journal for Numerical Methods in Fluids* 2006; **50**(7):817–844.
6. Sherman L, Taylor III AC, Green LG, Newman PA, Hou GW, Korivi VM. First- and second-order aerodynamic sensitivity derivatives via automatic differentiation with incremental iterative methods. *Journal of Computational Physics* 1996; **129**:307–331.
7. Lyness JN, Moler CB. Numerical differentiation of analytic functions. *SIAM Journal on Numerical Analysis* 1967; **4**(2):202–210.
8. Anderson WK, Newman JC, Whitfield DL, Nielsen EJ. Sensitivity analysis of Navier–Stokes equations on unstructured meshes using complex variables. *AIAA Journal* 2001; **39**(1):56–63.
9. Leclerc E, Sagaut P, Mohammadi B. On the use of incomplete sensitivities for feedback control of laminar vortex shedding. *Computers and Fluids* 2006; **35**(10):1432–1443.
10. Squire W, Trapp G. Using complex variables to estimate derivatives of real functions. *SIAM Review* 1998; **40**(1):110–112.
11. Lu SY, Sagaut P. Pseudo-characteristic formulation and dynamic boundary conditions for computational aeroacoustics. *International Journal for Numerical Methods in Fluids*, in press.
12. Sesterhenn J. A characteristic-type formulation of the Navier–Stokes equations for high order upwind schemes. *Computers and Fluids* 2001; **30**:37–67.
13. Zhuang M, Chen RF. Applications of higher-order optimized upwind schemes for computational aeroacoustics. *AIAA Journal* 2002; **40**(3):443–449.
14. Shu CW, Osher S. Efficient implementation of essentially non-oscillatory shock capturing schemes II. *Journal of Computational Physics* 1989; **83**:32–78.
15. Kovasznay LSG. Turbulence in supersonic flow. *Journal of the Aeronautical Society* 1953; **20**(10):657–682.

DOI: 10.1002/fld